Placement of virtual inertia from HVDC terminals based on a frequency deviation index

Paula B. Garcia-Rosa[1], Salvatore D'Arco[1], Jon Are Suul[1,2]

[1] *SINTEF Energy Research*, Trondheim, Norway

[2] *Department of Engineering Cybernetics, Norwegian University of Science and Technology*, Trondheim, Norway

E-mails: paula.garcia-rosa@sintef.no, salvatore.darco@sintef.no, Jon.A.Suul@sintef.no

Abstract—This paper presents an approach for assessing the most suitable locations to provide virtual inertia by HVDC converters. A frequency deviation index quantifying the maximum distance in Hz from each bus in the power system to the Center of Inertia (COI) is utilized as the starting point of the assessment. From this index, the buses that are exhibiting the largest relative frequency transients in response to power disturbances are identified as candidates for introducing virtual inertia. Then, the most suitable placement of virtual inertia contributions from existing HVDC terminals or alternative connection points for future HVDC links can be assessed. An example is presented by a simulation study based on a 44-bus simplified model of the Nordic power system implemented in DIgSILENT PowerFactory. This study shows how the overall transient behaviour of the frequency can be improved by operating an HVDC terminal as a Virtual Synchronous Machine (VSM) for providing virtual inertia to a bus with high frequency deviation index. The results also confirm how the VSM-based control can improve the frequency transients in terms of frequency nadir and rate-of-change-of-frequency.

Index Terms—Center of Inertia (COI), frequency transients, HVDC converters, inertia distribution, virtual inertia

I. INTRODUCTION

The recent increase in power generation from renewable energy sources with power electronic interfaces is causing growing concerns on the reduction of inertia in power systems. In Europe, this issue has become most critical for isolated power grids like the Irish and British transmission systems [1]–[4]. However, the combined effect from converter interfaced sources and decommissioning of traditional thermal power plants is also leading to challenges in large interconnected power systems. Thus, most transmission system operators are directing increasing attention towards future challenges related to inertia distribution and frequency regulation [5]–[7].

The operation of traditional large-scale power systems with a high share of generation from converter interfaced units is still a relatively new condition. However, the emerging challenges related to reduced equivalent inertia were predicted already at an early stage of the ongoing development towards distributed renewable power generation. Thus, strategies for providing virtual inertia from power electronic converters have been proposed since the early commercial introduction of variable speed wind turbines [8]–[10]. Indeed, the first proposals for providing virtual or synthetic inertia from wind turbines with doubly-fed induction generators were based on a transient power injection proportional to the derivative of the grid frequency. Such df/dt-based inertia emulation (IE) can be introduced as an auxiliary function of conventional "grid-following" control strategies [11]–[13]. Another general approach for providing virtual inertia is to explicitly emulate the power-balance-based synchronization mechanism of synchronous generators. This control approach can be generally referred to as a Virtual Synchronous Machine (VSM), as first introduced in [14], [15]. Such VSM-based control strategies require a more significant redesign of the control strategy for power electronic converters, but provide inherent capabilities for "grid-forming" operation [16].

Control of power converters for providing virtual inertia by df/dt-based or VSM-based approaches has been studied for a wide range of applications [13], [16]–[19]. Considering inertia emulation with "grid forming" capabilities, utilization of HVDC converter terminals can be of particular interest due to the high rating, which enables significant support to frequency regulation and islanding operations by a limited number of units. However, the location of units providing virtual inertia can significantly influence the frequency dynamics and the worst case transients in response to disturbances. Therefore, several recent studies have proposed methods for optimizing the placement of units intended for providing virtual inertia and transient frequency support [20]–[24]. Furthermore, an analytical study of a two-machine system has indicated that the highest impact of devices with IE functionality on inter-area oscillations is obtained when they are placed electrically the farthest away from the Center of Inertia (COI) [25]. On this basis, an index based on the integral of the squared differences between the frequency at a local bus and the COI frequency was proposed to estimate the electrical distance from the COI in large power systems [25].

Regardless of the methods applied for optimizing the location of virtual inertia in power systems, the resulting placement will rely on the network topology, the disturbance location, and the initial distribution of inertia in the system. Furthermore, in practical scenarios, the provision of virtual inertia from HVDC converter terminals will only be relevant at a limited number of specific buses in the power system.

In this paper, an approach based on the COI concept is applied to identify suitable locations for providing virtual inertia from HVDC converter terminals. Different from [25], the ℓ_∞-norm is proposed as an alternative metric to represent the electrical distance between a bus and the COI. In this way, the maximum frequency deviation of each bus from the COI is obtained, which gives an indication of the maximum impact from local oscillations. Then, this Frequency Deviation Index (FDI) has a direct and simple physical interpretation. The highest values of the FDI will indicate buses that are suitable candidates for introducing virtual inertia. An example of analysis is presented for a 44-bus model of the Nordic power system simulated in DIgSILENT PowerFactory. Based on an initial assessment of the system, it is shown how VSM-based control of an HVDC terminal and its location will affect the transient frequency behaviour. The results demonstrate how placement of virtual inertia at an HVDC bus with high FDI improves the overall transient behaviour of the frequency. This is reflected in an improved frequency nadir and a reduced Rate-of-Change-of-Frequency (RoCoF).

II. HVDC CONVERTER CONTROL

This study considers the problem of *where to place* the capability of providing virtual inertia from an HVDC converter, as will be discussed in Section III. The assumed approach for providing virtual inertia from the HVDC converter terminal is to apply VSM-based control. The implementation is based on the voltage controlled VSM introduced in [26], and adapted for an HVDC converter terminal in [27]. An overview of the control system is shown in Fig. 1. As indicated in the figure, the inertia emulation of this control strategy is provided by a virtual swing equation, which is defined by:

$$\frac{d\omega_{\text{VSM}}}{dt} = \frac{p^{r*}}{T_a} - \frac{p_o}{T_a} - \frac{k_d(\omega_{\text{VSM}} - \omega_{\text{PLL}})}{T_a}, \tag{1}$$

where T_a is the emulated inertia, k_d is the damping constant, and p_o is the measured output power from the converter terminal. The input power to the virtual swing equation (p^{r*}) is defined by a 'governor' function which, in this case, is a simple power/frequency droop:

$$p^{r*} = p_o^* + k_\omega(\omega^* - \omega_{\text{VSM}}). \tag{2}$$

The emulated inertial dynamics are defined by the virtual rotor speed ω_{VSM} according to (1), and by the corresponding phase angle θ_{VSM} resulting from the integral of ω_{VSM}. Thus, the virtual rotor position θ_{VSM} is defining the reference frame orientation of the control system and is used for all dq-transformations.

It should be noted that the Phase Locked Loop (PLL) shown in Fig. 1 is only utilized to detect the grid frequency ω_{PLL} for implementing the damping in (1). Thus, the PLL is not utilized for the grid synchronization of the control system, and the applied VSM-based control strategy is inherently designed for having grid forming functionality.

The control system in Fig. 1 includes an outer loop reactive power controller which provides the voltage amplitude for the inner loop control of the converter. A Virtual Impedance (VI) is included to ensure capability for stable operation in weak as well as strong grid conditions. For this purpose, a quasi-stationary VI representation is assumed:

$$\mathbf{v_o} = \hat{v}^{r*} - (r_{\text{VI}} - jx_{\text{VI}}) * \mathbf{i_o}, \tag{3}$$

where the bold symbols indicate vector representation of the dq quantities of voltages and currents.

The control functions of inertia emulation, power-frequency droop, and reactive power control are ensuring emulation of the general operational characteristics of a synchronous machine. In addition, the applied VSM implementation includes an inner loop dq-frame voltage controller which generates the references for an inner loop current controller. An active damping controller is also included to suppress potential LC-oscillations in the grid interface. Further details about the implementation and modelling of this VSM-based control system are available in [26]–[28]. Since only the dynamics on the ac-side are studied in this context, a conventional average model of a voltage source converter is utilized to represent the HVDC converter without considering the internal dynamics of modular multilevel converter-based terminals.

III. FREQUENCY DEVIATION WITH RESPECT TO THE CENTER OF INERTIA

An index for estimating the electrical distance of any bus in a power system from the COI was proposed in [25]. Following a power disturbance, the index for a bus k is defined by normalizing

$$S_d(k) = \int_T (f_k(t) - f_{\text{COI}}(t))^2 \, dt, \tag{4}$$

with respect to the highest S_d obtained for all buses, where

$$f_{\text{COI}}(t) = \frac{\sum_{j=1}^m H_j f_j(t)}{\sum_{j=1}^m H_j} \tag{5}$$

is the center of inertia frequency in Hz. Furthermore, f_k is the frequency at bus k, f_j and H_j are, respectively, the frequency and the inertia constant of the synchronous generator j, and m is the total number of generators. The index S_d (4) is evaluated over a predefined time interval of duration T.

After normalization, the indexes obtained from (4) range from 0 to 1 and are sorted from the lowest to the highest value [25]. The bus with the lowest index is interpreted as the closest bus to the COI and the bus with the highest index is the farthest from the COI. Numerical simulations have shown that this index is highly affected by the system topology and by several power system characteristics as the inertia of synchronous machines and the line parameters [29]. However, rather than indicating only if the buses are close or far from the COI, an index that quantifies how the frequency at each bus differs from the COI frequency immediately after a disturbance would also be of interest. This could give an indication of how large local oscillations are, while (4) does not provide a clear physical meaning for such purposes.
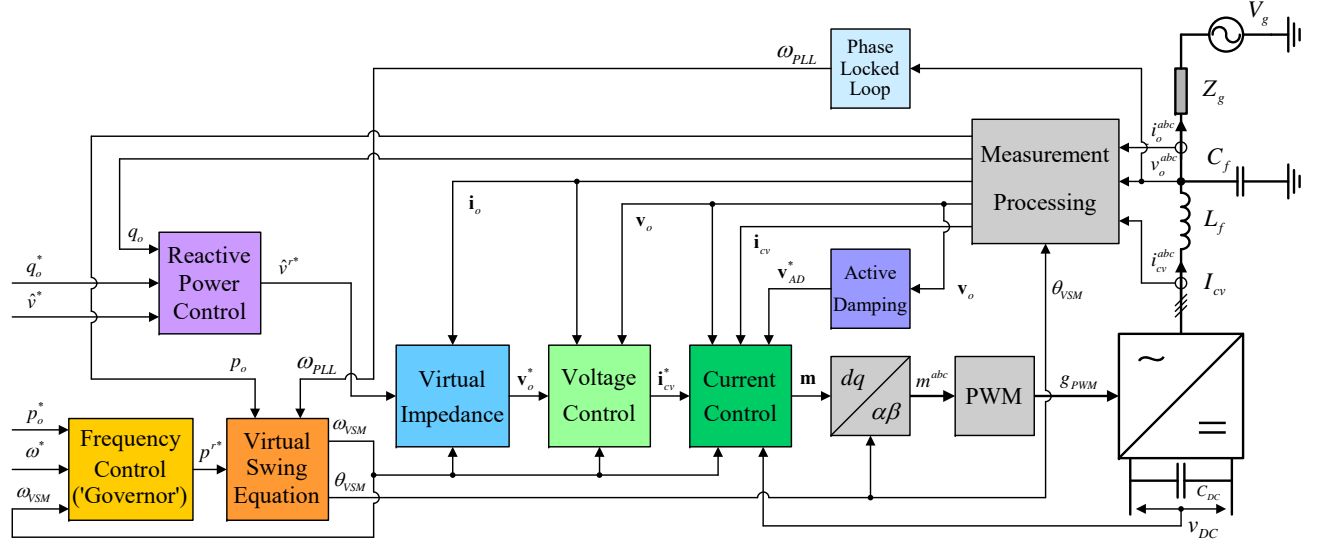
Fig. 1. Block diagram of the applied VSM-based control strategy for power-controlled HVDC terminal providing virtual inertia.

As a starting point for defining an alternative index of frequency deviation, consider a vector of distances d_k:

$$d_k = [f_{k,1} - f_{\text{COI},1}, f_{k,2} - f_{\text{COI},2}, \ldots, f_{k,n} - f_{\text{COI},n}]^\top, \quad (6)$$

with n samples corresponding to a time interval $T = n t_s$ within a power disturbance, where t_s is the sampling time in seconds. The ℓ_2-norm of (6) is calculated as:

$$L_d(k) := ||d_k||_2 = \left(\sum_{i=1}^{n} |d_{k,i}|^2 \right)^{1/2}, \quad (7)$$

which represents the distance over time between the local frequency and the COI frequency. Therefore, the metric (7) can be suitable for assessing the impact of oscillations in the local frequency with respect to the COI. However, it will not necessarily represent the worst case or maximum deviation of the local frequency, as would be critical for assessing the impact of virtual inertia support on the initial frequency transients after a disturbance. Thus, we define the frequency deviation index, FDI, of a bus k as the ℓ_∞-norm of the vector of distances (6), which gives the largest magnitude of distances in the vector. In this way, the ℓ_∞-norm for a bounded vector sequence d_k, here referred as $F_d(k)$,

$$F_d(k) := ||d_k||_\infty = \max_i |d_{k,i}|, \quad (8)$$

represents the maximum deviation of the frequency at bus k from the COI frequency (in Hz), after a power disturbance occurs in the system. By considering the maximum index ($F_{d,\max}$) obtained for all buses after a specific disturbance, the normalized index $\bar{F}_d(k)$ is given as the ratio $F_d(k)/F_{d,\max}$. Thus, normalized values suitable for graphical representation will range from 0 to 1, as in [25].

From the FDI defined by (8), the buses that are exhibiting the largest frequency transients in response to power disturbances are identified as candidates for introducing virtual inertia. As the provision of virtual inertia from HVDC converter terminals will only be relevant at a limited number of specific buses, the most suitable candidates are HVDC buses geographically closest to buses with the highest indexes or HVDC buses with the highest indexes.

IV. DESCRIPTION OF THE POWER NETWORK

The Nordic power system, consisting of the grid in Norway, Sweden, Finland and Eastern Denmark, is assumed as a reference case for assessing suitable locations of virtual inertia provided by HVDC terminals. The Nordic area is interconnected to central Europe with HVDC connections and an interconnection to United Kingdom is under construction. In this paper, the Nordic power system is modelled with a simplified representation with 44 buses, referred to as the Nordic 44-bus (N44) model [30]. This model includes 13 hydro-power stations and 5 thermal generation plants based on synchronous generators. Nine HVDC interconnections are included in the model, accounting for a transfer capacity of 3500 MW. An overview of the N44 model is displayed in Fig. 2, and has been implemented in DIgSILENT PowerFactory as a quasi-stationary phasor model.

Since this study focuses on the frequency dynamics, the inertia and the governor of the generators have been calibrated to reproduce responses comparable to what has been observed in the actual Nordic power system. Table I shows a comparison of the peak frequency transient obtained from the N44 model with real values shown in [7], after trips in the power system.
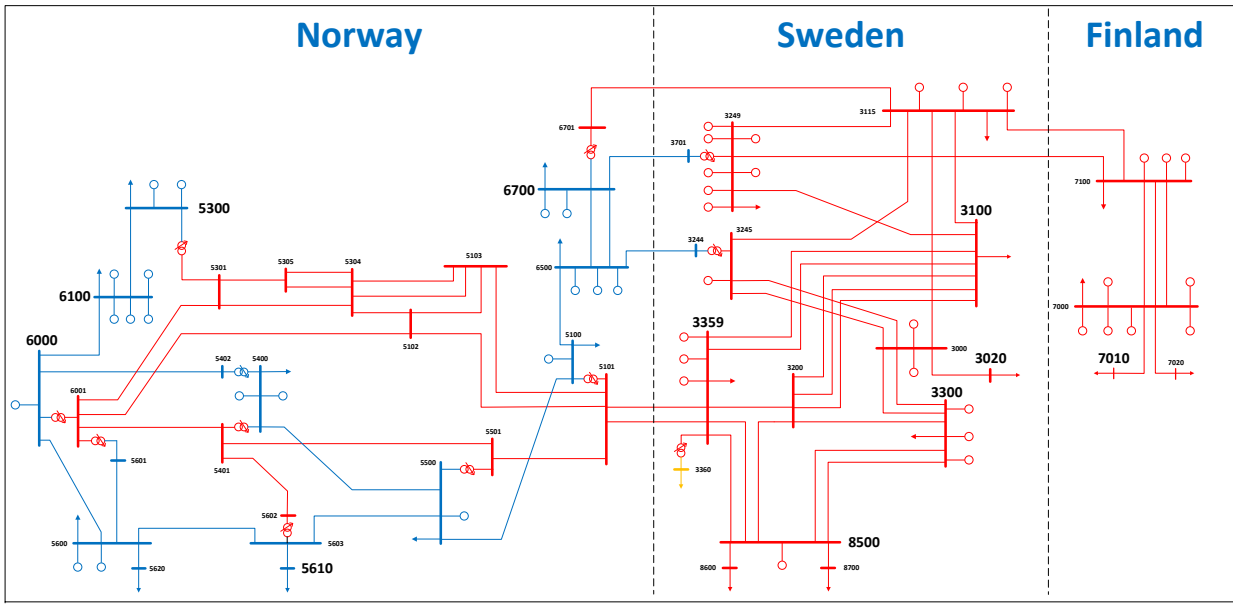
Fig. 2. Overview of the Nordic 44-bus power system model.

TABLE I
COMPARISON OF MINIMUM/MAXIMUM FREQUENCY VALUES (IN HZ)
OBTAINED FROM N44 WITH REAL VALUES AS SHOWN IN [7]

Trip of	Simulation results from N44	Real values as in [7]
Line in South-Eastern Norway	49.61	49.63
HVDC link at bus 5620	50.34	50.35
HVDC link at bus 7020	50.12	50.18

V. SIMULATION RESULTS

Simulation results are initially presented to illustrate the behavior of the FDI (8) for the Nordic 44-bus model. In this case, all HVDC connections are modeled as loads. Finally, section V-B presents simulation results including a point-to-point HVDC connection with one terminal controlled as a VSM for inertia emulation. The objective is to verify the effect of placing virtual inertia from HVDC links according to the obtained results for the FDI in the N44 model.

A. Frequency Deviation Index on the Nordic 44 Bus Model

Fig. 3.a shows how the FDI is distributed within the N44 model when a load step disturbance of $700\,\mathrm{MW}$ occurs in bus 6100 at 1 s. In this case, the farthest bus from the COI is the bus where the disturbance occurs. Furthermore, the region with the buses farthest from the COI, i.e. where $F_d \geq 0.75\,F_{d,\max}$, includes bus 5300, which is in the neighborhood of 6100 in Norway (as illustrated in Fig. 2). The region with the buses closest to the COI, i.e. $F_d \leq 0.25\,F_{d,\max}$, includes buses in Sweden: 3100, 3359 (central nodes) and 8500, which is connected to the synchronous machine with the largest inertia constant. Fig. 3.a also indicates the location of HVDC terminals in the N44. The frequency behaviour for the buses closest to and farthest away from the COI is illustrated in
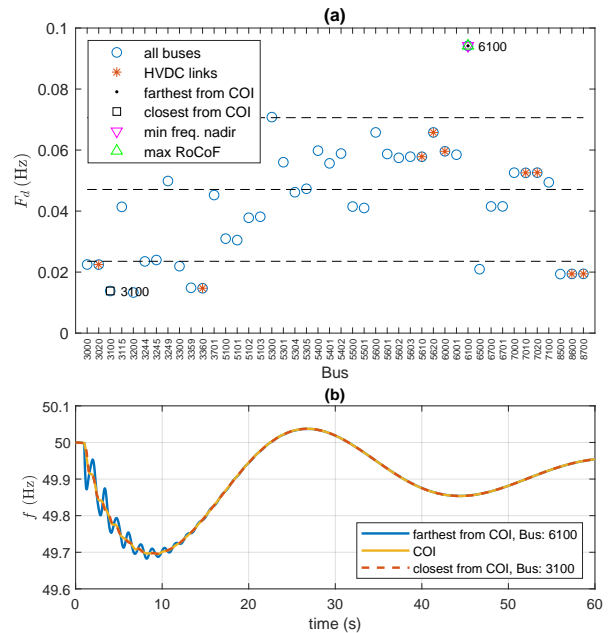

Fig. 3. Localized disturbance of $700\,\mathrm{MW}$ at bus 6100. (a) FDI (horizontal lines indicate, from the bottom to the top, $0.25\,F_{d,\max}$, $0.5\,F_{d,\max}$ and $0.75\,F_{d,\max}$); (b) frequency in bus 6100, COI, and bus 3100.

Fig. 3.b. It can be noted that bus 6100 exhibits inter-area oscillations while bus 3100 has a smoother transient when compared to the COI frequency.

An FDI map for a localized disturbance of $700\,\mathrm{MW}$ at different load buses is shown in Fig. 4.a. The x-axis represents the disturbed buses, while the y-axis represents all 44 buses of the power network. The disturbances have occurred at different instants of time in all buses with connected loads, except
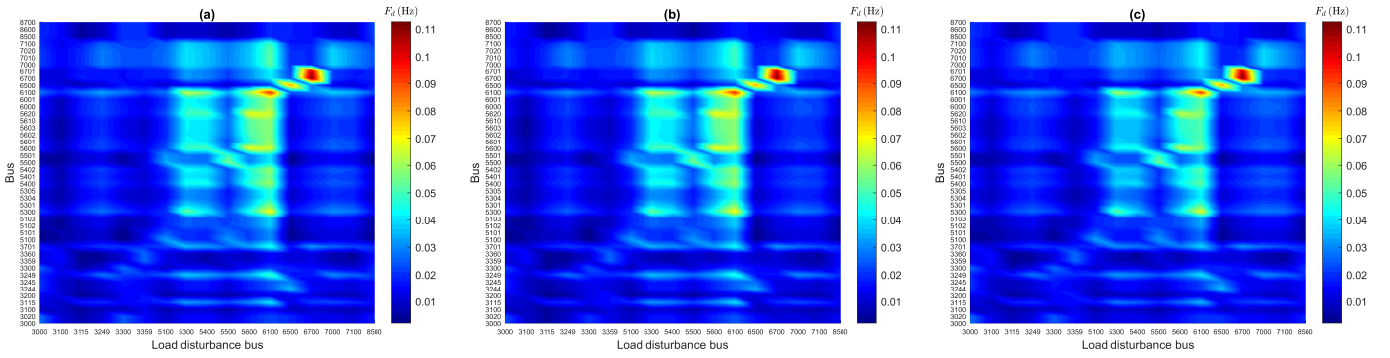
Fig. 4. FDI map for localized disturbances of 700 MW: (a) initial system; (b) virtual inertia placed at bus 3020; and (c) virtual inertia placed at bus 6000.
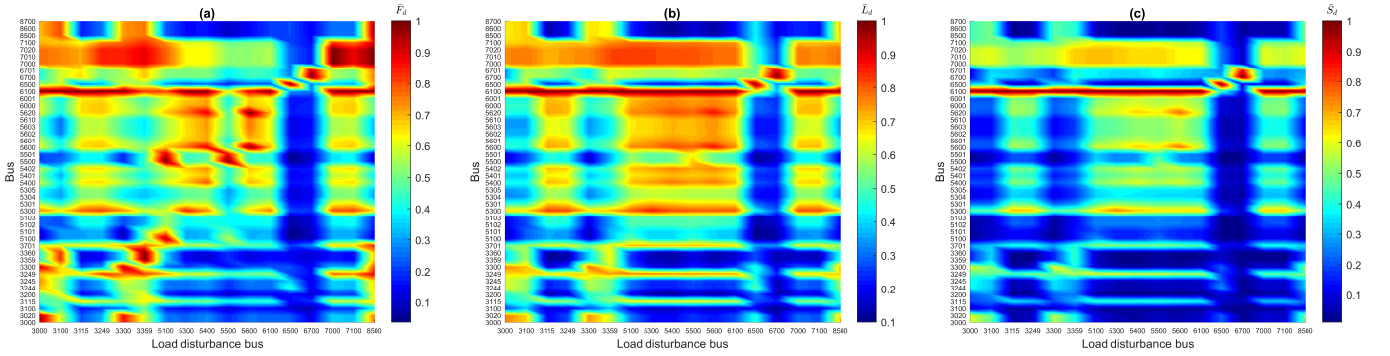

Fig. 5. Normalized maps for localized disturbances of 700 MW for the initial system: (a) FDI; (b) normalization of L_d; and (c) normalization of S_d.

HVDC buses. The highest values of the FDI corresponding to the largest deviations from the COI are observed for a load disturbance either at 6100 or 6700. Furthermore, the normalized FDI map in Fig. 5.a illustrates for which cases a bus acts as weak or strong node, i.e. far from or close to the COI. For instance, 3000 and 3300 are weak nodes only when the disturbance is at the bus or in its neighborhood (e.g., at 3100, 3359, 8500). However, peripheral buses like 5300 and 6100 are more frequently far from the COI. The normalized map also shows that while bus 6100 is the weakest node for most of the disturbances, 6700 has the largest deviations from the COI only when the disturbance is at this bus.

Fig. 5.b and Fig. 5.c show the map for normalized values of metrics from (7) and (4), respectively. Since both metrics penalize large deviations over the interval, buses with the largest deviations (e.g. 6100 and 6700) have a much higher index than others after normalization. The difference with respect to Fig. 5.a is lower for Fig. 5.b than for Figs. 5.c due to the square root operation of the ℓ_2-norm. In contrast to (4) and (7), (8) indicates only the maximum deviation without any weighing. Therefore, the map in Fig. 5.a highlights that a bus is often far from the COI when there is a disturbance at the bus itself or around its neighborhood.

B. Placement of Virtual Inertia provided by HVDC converters

This section verifies the impact of placing virtual inertia from an HVDC link according to the FDIs obtained for the

N44 model. The buses with HVDC terminals geographically closest to buses exhibiting the largest frequency deviations according to the FDI are initially identified as the most suitable candidates for introducing virtual inertia.

For all the simulation results, the HVDC interconnection with one terminal controlled as the VSM is based on the planned Nordlink interconnection, which is a bipolar HVDC link rated at 1500 MVA $\pm$525 kV dc, modelled as described in [27]. The converters are connected through grid-side filters and transformers to the N44 network in one side, and to an equivalent ac voltage source representing a simplified strong grid in the other side. The main parameters of the HVDC configuration and VSM-based control are shown in Table II.

Simulation results obtained for the frequency deviation index in section V-A showed that the bus 6100 is the node with the largest deviations from the COI bus for most of the load disturbance cases. Geographically, the closest bus to 6100

TABLE II
MAIN SIMULATION PARAMETERS HVDC AND VSM-BASED CONTROL

Parameter	Value	Parameter	Value
Rated ac voltage	285 kV	Rated grid frequency	50 Hz
Frequency droop gain (k_ω)	20 pu	Filter capacitance	0.074 pu
VSM damping factor (k_d)	150 pu	Filter inductance	0.08 pu
VSM inertia constant (T_a)	10 s	Filter resistance	0.003 pu

with an HVDC link is bus 6000, where the North Sea Link will be constructed to connect the electricity systems of Norway and UK. Thus, the VSM-based control is initially implemented at this HVDC converter terminal.

To illustrate how the FDI is affected by introducing virtual inertia at different locations, Fig. 4.c and Fig. 4.b show the FDI map for localized disturbances of 700 MW when the HVDC link at bus 6000 or 3020 is controlled as a VSM. It should be noted that prior to each load disturbance, the system is operating in steady-state conditions with a power transfer of 750 MW (0.5 pu) through the VSM-controlled HVDC link. When compared to the initial system (Fig. 4.a), the FDI at the central area of the map (load disturbance bus from 5100 to 6100) is reduced when the VSM is at bus 6000. However, there is no clear difference in the same area when the VSM is located at bus 3020, since this node is affected mainly by disturbances in its neighborhood (as shown in Fig. 5.a). In addition, it has been verified that the largest deviations at buses 6100 and 6700 are respectively reduced by 15% and 21%, when virtual inertia are placed exactly at the buses.

Finally, Fig. 6 and Fig. 7 illustrate the effect on the time response by providing virtual inertia from an HVDC terminal at different locations. The figures show the transient behaviour of the frequency and the output power from the converter terminal, when load step disturbances of 2200 MW are applied at buses 6100 and 3300. For the disturbance at bus 6100 (Fig. 6), placing the virtual inertia at either 5610 or 6000 results in smoother transient than placing at other nodes. When the disturbance is at bus 3300 (Fig. 7), placing the virtual inertia at the HVDC bus 3020 results in slightly smaller frequency deviation than at 6000. As illustrated in Fig. 5.a, the bus 3020 has higher FDI than bus 6000 and it is also closer to the disturbed bus.

Table III shows the maximum observed values of RoCoF and frequency deviation at the nadir for all 44 buses, including results for the initial system without virtual inertia. A comparison of maximum values obtained for the FDI and the ℓ_2-norm (L_d) is also shown. Although the FDI is reduced only when the placement is at buses electrically farther from the COI and geographically closer to the disturbance bus, inspection of the ℓ_2-norm shows that the overall transient behaviour improves. In all cases with virtual inertia provided by the HVDC terminal, the frequency nadir is improved compared to the initial system. In particular, when the disturbance occurs at bus 6100, the VSM at 6000 results in nadir and RoCoF very close to the lowest values, which are obtained when the VSM is at 5610. The frequency deviation at the nadir and the RoCoF are improved about 9% and 20%, respectively, when compared to other allocations. When the disturbance occurs at bus 3300, the corresponding improvements by placing the VSM at bus 3020 are about 6% and 34%, respectively.

VI. CONCLUSIONS

This paper introduced a frequency deviation index (FDI) as a metric to quantify the distance of a bus from the center of inertia during a frequency disturbance in the power system.
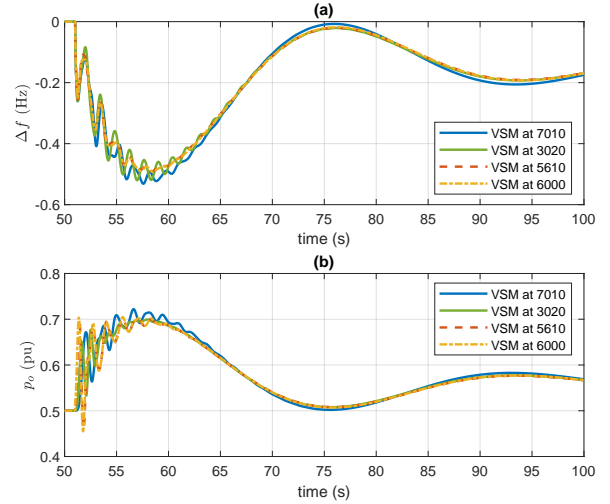

Fig. 6. Localized disturbance of 2200 MW at bus 6100: (a) frequency deviation (Δf) from nominal value; (b) output power from the converter positive terminal.
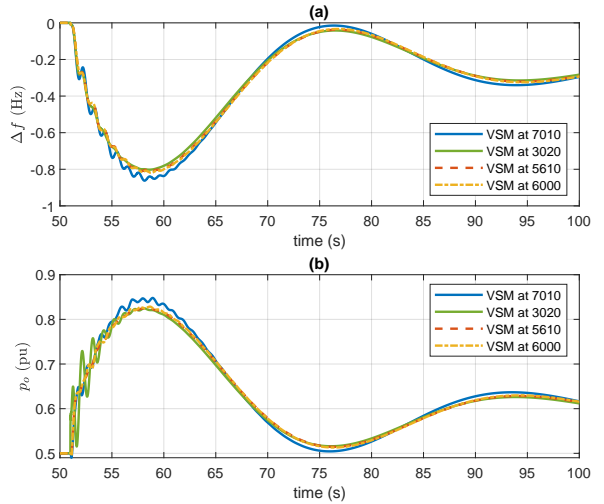

Fig. 7. Localized disturbance of 2200 MW at bus 3300: (a) frequency deviation (Δf) from nominal value; (b) output power from the converter positive terminal.

TABLE III
MAXIMUM VALUES OF FREQUENCY DEVIATION AT NADIR (HZ), ROCOF (HZ/S), FDI (HZ), AND L_d (HZ) OBSERVED FOR ALL 44 BUSES AFTER A LOAD STEP DISTURBANCE OF 2200 MW

Load step	Metric	Initial system	VSM at 7010	VSM at 3020	VSM at 5610	VSM at 6000
Bus 6100	Δf_{nadir}	0.958	0.806	0.780	0.732	0.736
	RoCoF	1.014	0.971	1.078	0.852	0.860
	FDI	0.285	0.284	0.285	0.284	0.281
	L_d	2.137	2.110	2.050	1.761	1.720
Bus 3300	Δf_{nadir}	1.020	0.864	0.805	0.821	0.825
	RoCoF	0.312	0.323	0.242	0.363	0.367
	FDI	0.090	0.101	0.082	0.093	0.094
	L_d	0.960	1.159	0.629	0.861	0.837

This index can be applied to identify the weakest nodes in the power system from a frequency regulation perspective and the locations where inertia support is most beneficial for limiting the maximum local frequency deviation. In a planning phase, the frequency deviation index could be applicable to evaluate the possible benefits from inertia support on candidate buses for the connections of an HVDC terminal. In an operating phase, the index can be beneficial to assess which terminal is most suitable for introducing virtual inertia.

The proposed FDI metric was evaluated by numerical simulations for assessing the placement of virtual inertia provided by an HVDC terminal in a simplified representation of the Nordic power system. The resulting FDI map shows the impact of disturbances located at different buses and can be useful for indicating the magnitude of local transients, while a map with the normalized indexes can indicate in which cases a bus will be electrically far or close from the COI. The latter clearly outlines that a bus is often far from the COI when there is a disturbance at the bus itself or around its neighborhood. However, this is not the only case when a bus is far from the COI. For instance, numerical simulations with the N44 model showed that bus 6100 in Norway is the farthest from the COI for most of the load disturbances, regardless of the disturbance location. Furthermore, preliminary results showed that by placing virtual inertia at an HVDC bus with high FDI and geographically close to disturbance, the overall transient behaviour of the frequency is improved, which is also reflected in an improved frequency nadir and a reduced RoCoF.

REFERENCES

[1] J. O'Sullivan, A. Rogers, D. Flynn, P. Smith, A. Mullane, and M. O'Malley, "Studying the maximum instantaneous non-synchronous generation in an island system – Frequency stability challenges in ireland," *IEEE Trans. on Power Syst.*, vol. 29, no. 6, pp. 2943–2951, 2014.

[2] M. Yu, A. Dysko, C. Booth, A. Roscoe, J. Zhu, and H. Urdal, "Investigations of the constraints relating to penetration of non-synchronous generation (NSG) in future power systems," in *Proc. of the 6th Protection, Automation and Control World Conf. (PAC World 2015)*, 2015.

[3] M. Yu, A. J. Roscoe, A. Dyśko, C. D. Booth, R. Ierna, J. Zhu, and H. Urdal, "Instantaneous penetration level limits of non-synchronous devices in the British power system," *IET Renewable Power Generation*, vol. 11, no. 8, pp. 1211–1217, 2016.

[4] M. Nedd, W. Bukhsh, C. MacIver, and K. Bell, "Metrics for determining the frequency stability limits of a power system: a GB case study," *Electric Power Systems Research*, vol. 190, no. 106553, 2020.

[5] B. Hartmann, I. Vokony, and I. Táczi, "Effects of decreasing synchronous inertia on power system dynamics – Overview of recent experiences and marketisation of services," *Int. Transactions on Electrical Energy Systems*, vol. 29, no. 12, p. e12128, 2019.

[6] Y. Wang, H. Silva-Saravia, and H. Pulgar-Painemal, "Actuator placement for enhanced grid dynamic performance: A machine learning approach," *IEEE Trans. on Power Syst.*, vol. 34, no. 4, pp. 3119–3128, 2019.

[7] E. Ørum, M. Kuivaniemi, M. Laasonen, A. I. Bruseth, E. A. Jansson, A. Danell, K. Elkington, and N. Modig, "Future system inertia," *ENTSO-E, Brussels, Tech. Rep*, 2015.

[8] J. Ekanayake and N. Jenkins, "Comparison of the response of doubly fed and fixed-speed induction generator wind turbines to changes in network frequency," *IEEE Transactions on Energy conversion*, vol. 19, no. 4, pp. 800–802, 2004.

[9] J. Morren, S. W. De Haan, W. L. Kling, and J. Ferreira, "Wind turbines emulating inertia and supporting primary frequency control," *IEEE Trans. on Power Syst.*, vol. 21, no. 1, pp. 433–434, 2006.

[10] J. Morren, J. Pierik, and S. W. De Haan, "Inertial response of variable speed wind turbines," *Electric power systems research*, vol. 76, no. 11, pp. 980–987, 2006.

[11] A. Vassilakis, P. Kotsampopoulos, N. Hatziargyriou, and V. Karapanos, "A battery energy storage based virtual synchronous generator," in *Proc. of the IREP Symp. Bulk Power System Dynamics and Control-IX Optimization, Security and Control of the Emerging Power Grid*, 2013, pp. 1–6.

[12] D. Duckwitz and B. Fischer, "Modeling and design of df/dt-based inertia control for power converters," *IEEE Journal of Emerging and Selected Topics in Power Electron.*, vol. 5, no. 4, pp. 1553–1564, 2017.

[13] E. Rakhshani and P. Rodriguez, "Inertia emulation in ac/dc interconnected power systems using derivative technique considering frequency measurement effects," *IEEE Transactions on Power Systems*, vol. 32, no. 5, pp. 3338–3351, 2016.

[14] H.-P. Beck and R. Hesse, "Virtual synchronous machine," in *Proc. of the 9th Int. Conf. on Electrical Power Quality and Utilisation*, 2007, pp. 1–6.

[15] Y. Chen, R. Hesse, D. Turschner, and H.-P. Beck, "Dynamic properties of the virtual synchronous machine (VISMA)," *Proc. ICREPQ*, vol. 11, 2011.

[16] S. D'Arco and J. A. Suul, "Virtual synchronous machines - Classification of implementations and analysis of equivalence to droop controllers for microgrids," in *Proc. of the IEEE Grenoble Conf.*, 2013, pp. 1–7.

[17] M. Guan, W. Pan, J. Zhang, Q. Hao, J. Cheng, and X. Zheng, "Synchronous generator emulation control strategy for voltage source converter (VSC) stations," *IEEE Transactions on Power Systems*, vol. 30, no. 6, pp. 3093–3101, 2015.

[18] J. Zhu, C. D. Booth, G. P. Adam, and A. J. Roscoe, "Inertia emulation control of VSC-HVDC transmission system," in *Proc. of the Int. Conf. on Advanced Power System Automation and Protection*, 2011, pp. 1–6.

[19] J. Fang, H. Li, Y. Tang, and F. Blaabjerg, "On the inertia of future more-electronics power systems," *IEEE Journal of Emerging and Selected Topics in Power Electronics*, vol. 7, no. 4, pp. 2130–2146, 2018.

[20] B. K. Poolla, S. Bolognani, and F. Dörfler, "Optimal placement of virtual inertia in power grids," *IEEE Transactions on Automatic Control*, vol. 66, no. 12, pp. 6209–6220, 2017.

[21] T. S. Borsche, T. Liu, and D. J. Hill, "Effect of rotational inertia on power system damping and frequency transients," in *Proc. of the 54th IEEE Conf. on Decision and Control (CDC)*, 2015.

[22] N. Hariyanto, L. Chao-Yuan, L. Chih-Wen *et al.*, "Optimal placement of energy storage with synthetic inertia control on a grid with high penetration of renewables using mean-variance mapping optimization," in *Proc. of IEEE PES Asia-Pacific Power and Energy Engineering Conf. (APPEEC)*, 2019, pp. 1–6.

[23] W. J. Farmer and A. Rix, "Optimising power system frequency stability using virtual inertia from inverter-based renewable energy generation." in *Proc. of the Int. Conf. on Clean Electrical Power (ICCEP)*, 2019, pp. 394–404.

[24] B. K. Poolla, D. Groß, and F. Dörfler, "Placement and implementation of grid-forming and grid-following virtual inertia and fast frequency response," *IEEE Trans. on Power Syst.*, vol. 34, no. 4, pp. 3035–3046, 2019.

[25] H. Pulgar-Painemal, Y. Wang, and H. Silva-Saravia, "On inertia distribution, inter-area oscillations and location of electronically-interfaced resources," *IEEE Trans. on Power Syst.*, vol. 33, no. 1, pp. 995–1003, 2018.

[26] S. D'Arco, J. A. Suul, and O. B. Fosso, "Small-signal modelling and parametric sensitivity of a virtual synchronous machine," in *Proc. of the Power Systems Computation Conf.*, 2014, pp. 1–9.

[27] F. Palombi, L. Piegari, S. D'Arco, A. G. Endegnanew, and J. A. Suul, "Impact on power system frequency dynamics from an HVDC transmission system with converter stations controlled as virtual synchronous machines," in *Proc. of IEEE Milan PowerTech*, 2019, pp. 1–6.

[28] S. D'Arco, J. A. Suul, and O. B. Fosso, "A virtual synchronous machine implementation for distributed control of power converters in smartgrids," *Electric Power Systems Research*, vol. 122, pp. 180–197, 2015.

[29] Y. Wang, H. Silva-Saravia, and H. Pulgar-Painemal, "Estimating inertia distribution to enhance power system dynamics," in *Proc. of the North American Power Symp. (NAPS)*, Morgantown, WV, 2017.

[30] S. H. Jakobsen, L. Kalemba, and E. H. Solvang, "The Nordic 44 test network," *figshare*, 2018, https://doi.org/10.6084/m9.figshare.7464386.v1.